Nuclear Science and Techniques (2025) 36:76
https://doi.org/10.1007/s41365-025-01653-z

Electronic thermal conductivity of tungsten-based systems during collision cascade processes

Jiong-Rong Wang[1] · Bi-Cai Pan[1,2]

Received: 12 January 2024 / Revised: 15 April 2024 / Accepted: 13 May 2024 / Published online: 20 March 2025

Abstract

The thermal conductivity of plasma-facing materials (PFM) exposed to intense radiation is a critical concern for the reliable usage of materials in fusion reactors. However, limited research has been performed regarding the thermal conductivity of structures that rapidly change in a short time during collision cascade processes under irradiation. In this study, we employed the tight-binding (TB) method to investigate the electronic thermal conductivity (κ_e) of tungsten-based systems during various cascading processes. We found that κ_e values sharply decrease within the initial 0.3 picoseconds and then partially recover at a slow pace; this is closely linked to the evolution of defects and microstructural distortions. The increase in the initial kinetic energy of the primary knock-on atom and the presence of a high concentration of hydrogen atoms further decrease the κ_e values. Conversely, higher temperatures have a significant positive effect on κ_e. Furthermore, the presence of a grain boundary $\sum 5[001](130)$ substantially reduces κ_e, whereas the absorption effect of point defects by the grain boundary has little influence on κ_e during cascades. Our findings provide a theoretical basis for evaluating changes in the thermal conductivity performance of PFMs during their usage in nuclear fusion reactors.

Keywords Electronic thermal conductivity · Collision cascade · Tungsten · Plasma-facing materials · Tight-binding calculations

1 Introduction

In fusion reactors, excellent thermal transport properties are crucial for the regular service of plasma-facing materials (PFMs), which suffer from steady and transient heat loads. As a primary PFM candidate, tungsten (W) crystals have good thermal conductivity (κ), but significant degradation of κ is inevitable owing to the drastic increase in defect density under high-dose irradiation from the plasma [1–4]. Specifically, during high-energy neutron irradiation, collisions between neutrons and lattice atoms trigger cascade processes, leading to the production of numerous point defects in the PFM on femtosecond timescales [5]. These point defects then recombine or evolve into extended defects, resulting in severe material damage, such as swelling and hardening [6]. Throughout the irradiation process, the κ value changes with the drastic structural alteration. Experiments measuring κ after irradiation have demonstrated that the κ of W samples decreases with increasing irradiation dosage, whereas high temperatures capable of inducing significant dynamic annealing in W can partially restore κ [7–10]. However, real-time experimental measurement of κ during irradiation remains challenging, despite the ability to directly observe the evolution of defects in situ [11–13]. Therefore, computer simulations are necessary to study the behavior of κ during irradiation under various conditions.

To date, most theoretical studies have used classical molecular dynamics (MD) methods employing a primary knock-on atom (PKA) to investigate complex structures under different cascade conditions. These studies explored the effects of the kinetic energy of the PKA, temperature

This work was supported by the Collaborative Innovation Program of Hefei Science Center of CAS (No. 2022HSC-CIP007).

✉ Bi-Cai Pan
bcpan@ustc.edu.cn

[1] Key Laboratory of Strongly-Coupled Quantum Matter Physics, Department of Physics, University of Science and Technology of China, Hefei 230026, China

[2] Hefei National Laboratory for Physical Sciences at Microscale, University of Science and Technology of China, Hefei 230026, China

[14], and the presence of helium atoms [15] on the surviving defects in tungsten systems. As the PKA energy increases or interstitial helium atoms are introduced, the number of surviving defects increases, whereas the temperature has little effect on the defects. Additionally, there has been significant interest in understanding the influence of grain boundaries (GBs) during cascades, as GBs can act as effective sinks for point defects and exhibit a bias-absorption effect on interstitials [16–22]. These studies have succeeded in obtaining complex structures during cascade processes, whereas few models can predict the thermal conductivities of such intricate atomistic configurations [18], particularly for structures arising during cascade processes in which drastic structural changes occur in an extremely short period. Consequently, most thermal conductivity calculations rely on structures that have reached steady states, allowing researchers to explore only the effects of various types of irradiation-induced defects on thermal conductivities or post-cascade changes in the thermal conductivities [23–29]. In tungsten systems, the lattice thermal conductivity decreases in the presence of voids or GBs, with a further reduction when these defects trap significant amounts of helium or hydrogen atoms. The overall thermal conductivity κ decreases in the presence of GBs and further decreases when the GBs are covered by voids. Additionally, the introduction of the impurity rhenium also reduces κ. Furthermore, it is worth noting that the majority of research on metal W has focused on lattice thermal conductivity using non-equilibrium molecular dynamics simulations [25–27] and the overall thermal conductivity based on the phase-field model [23, 24], whereas research on the electronic thermal conductivity (κ_e) that dominates metal thermal transport is relatively limited.

In this study, we employed a tight-binding (TB) potential model developed for W-based systems [30] to simulate cascade processes and calculate the corresponding κ_e at the quantum theory level. We accounted for the effects of PKA energy, temperature, the presence of hydrogen (H) atoms, and the presence of a GB on the κ_e of W systems during cascades.

2 Methods

In this study, cascade simulations and calculations of κ_e were performed based on the developed WHTB model [30], where the Hamiltonian matrix of each system is parameterized to handle large-scale systems within the framework of quantum mechanics. For our investigations into the effects of low-energy PKA, H atoms, and temperature on κ_e, we applied a $9 \times 9 \times 14$ supercell consisting of 2268 W atoms (Fig. 1a). To study the effect of the GB, we constructed a common symmetric tilt GB structure, $\sum 5[001](130)$, with

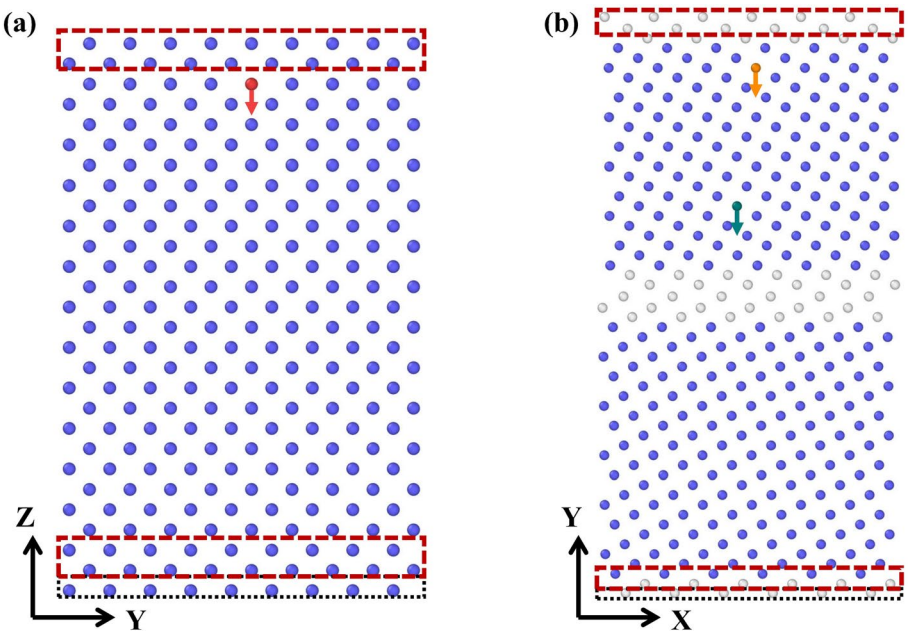

Fig. 1 (Color online) Schematic diagrams of pure tungsten system (**a**) and tungsten system containing the GB (**b**). The blue spheres represent atoms with body-centered cubic structural features. The white spheres represent atoms with other structural features, which can be considered as atoms forming the GB. The red, green, and yellow spheres represent the PKA atoms that we chose, and the corresponding arrows represent the incident directions. Atoms in black dashed boxes were fixed, and those in red dashed boxes represent thermostat regions. For the pure tungsten system, X=[100], Y=[010], and Z=[001]. For the GB system, Z=[001], and for the grain in the upper half, X=[3-10] and Y=[130], while for the grain in the lower half, X=[310] and $Y = [-130]$

a size of $3\sqrt{10}\times 6\sqrt{10}\times 8$, composed of 2832 W atoms (Fig. 1b).

To achieve thermodynamic equilibrium states, we conducted tight-binding molecular dynamics (TBMD) simulations of up to 5-8 picoseconds (ps) at the NPT ensemble (N represents the number of particles, P represents pressure, and T represents temperature) for the considered systems. Then, to simulate the cascade processes, the atomic layer at the bottom of the supercell was fixed to prevent system translation, and four atomic layers (two at the bottom and two at the top) were used as thermostat regions to control the temperature of the simulation system using the Berendsen temperature control technique [31]. For general systems (Fig. 1a), the PKA was chosen beneath the top thermostat region, and the incident direction was in the negative Z direction. Regarding the GB systems, two PKAs at different distances from the GB were selected, with the incident direction perpendicular to the GB along the negative Y direction (Fig. 1b). Additionally, we adopted an adaptive time-stepping scheme based on the method proposed by Nordlund [32] and set a maximum step time of 1 fs. To obtain the statistical average results, we performed three sets of cascade simulations under different conditions.

Furthermore, we extracted the structures at different times during the cascades and calculated their κ_e values. The Kubo-Greenwood method was used to obtain κ_e values, and the average electron mean free path (MFP) was calculated to evaluate the strength of electron scattering. In our theoretical approach, based on the Kubo formula [33–35] and the Chester-Tellung version of the Kubo-Greenwood formula [36, 37], κ_e can be obtained as follows:

$$\kappa_e = \frac{1}{e^2 T}\left(L_{22} - \frac{L_{12}^2}{L_{11}}\right), \tag{1}$$

$$L_{ij} = (-1)^{i+j}\int \sigma(E)\left(E - E_f\right)^{i+j-2}\left(-\frac{\partial f(E)}{\partial E}\right)\mathrm{d}E, \tag{2}$$

$$\sigma_{\alpha\alpha} = -\frac{2i\hbar}{V}\sum_{\boldsymbol{k}}\sum_{m\neq n}\frac{f\left(\varepsilon_n(\boldsymbol{k})\right) - f\left(\varepsilon_m(\boldsymbol{k})\right)}{\varepsilon_n(\boldsymbol{k}) - \varepsilon_m(\boldsymbol{k})}\times \frac{\langle n\boldsymbol{k}|\mathrm{J}_\alpha|m\boldsymbol{k}\rangle\langle m\boldsymbol{k}|\mathrm{J}_\alpha|n\boldsymbol{k}\rangle}{\varepsilon_n(\boldsymbol{k}) - \varepsilon_m(\boldsymbol{k}) + i\eta}(\alpha = x, y, z). \tag{3}$$

where T in formula (1) is the absolute temperature, E_f in formula (2) is the Fermi level, $f(E)$ is the Fermi-Dirac distribution function, and $\sigma(E)$ is the DC electrical conductivity corresponding to energy E at $T = 0$ K, which can be obtained from formula (3). In formula (3), $\varepsilon_n(\boldsymbol{k})$ and $|n\boldsymbol{k}\rangle$ are the eigenvalue and the related eigenvector corresponding to the wavevector $\boldsymbol{k}$ in the Brillouin zone, respectively, obtained using the TB method. V is the volume of the calculated system, J_α is the current operator along the α direction, η is a positive real number, and the real part of $\sigma_{\alpha\alpha}$ is the DC electrical conductivity. The average electron MFP can be calculated using the following formula [38, 39]:

$$\langle l_e\rangle = \frac{\int \frac{D_{\max}(E)}{v(E)}\rho(E)\left(-\frac{\partial f}{\partial E}\right)\mathrm{d}E}{\int \rho(E)\left(-\frac{\partial f}{\partial E}\right)\mathrm{d}E}, \tag{4}$$

where $D_{\max}(E)$ is the maximum value of the diffusion coefficient, which can be obtained from the Einstein relation [40] using $\sigma(E)$ and the electronic density of states per unit volume $\rho(E)$. $v(E)$ is the effective group velocity of the electrons at energy E.

In addition, we counted the defects in the systems, including displaced atoms (with a displacement exceeding half the nearest-neighbor distance) and Frenkel pairs (identified using the Wigner-Seitz cell method [41]), and evaluated the centrosymmetry parameters (CSPs) of the atoms to understand the change in κ_e from the perspective of the structure. The CSP is defined as $P = \sum_{i=1,4}\left|\mathbf{R}_i + \mathbf{R}_{i+4}\right|^2$ for each atom in body-centered cubic structures, where $\mathbf{R}_i$ and $\mathbf{R}_{i+4}$ are the vectors or bonds corresponding to the four pairs of opposite nearest neighbors [42]. A larger P value indicates a greater departure from centrosymmetry in the immediate vicinity of the given atom. To evaluate the deviation of the entire structure from centrosymmetry, we counted the number of atoms with P values exceeding 1 and summed their P values (marked as Psum). Additionally, we calculated the rate of change of Psum by dividing the difference between Psum at a given time and Psum at 0 ps by Psum at 0 ps.

3 Results and discussion

3.1 Effects of PKA energies and H atoms on electronic thermal conductivity

The calculations in this section were performed at 800 K, which is the operating temperature for W-PFM. Figure 2a illustrates the variation in κ_e values for pure tungsten systems during cascades, where the initial kinetic energy of PKA (represented as E_{PKA}) is 300 eV and 500 eV, respectively. It is evident that κ_e undergoes a significant decrease during the initial stage (approximately 0.3 ps), followed by a partial recovery at a slow pace. As E_{PKA} increases, κ_e further decreases during the initial stage, whereas the recovery rate remains almost unchanged during the recovery period. In addition, it should be noted that even after approximately 4 ps, κ_e values for cases with E_{PKA} values of 300 eV and 500 eV recover to only approximately 64% and 55% of the pristine crystal's value, respectively. We will provide a discussion of this phenomenon later.

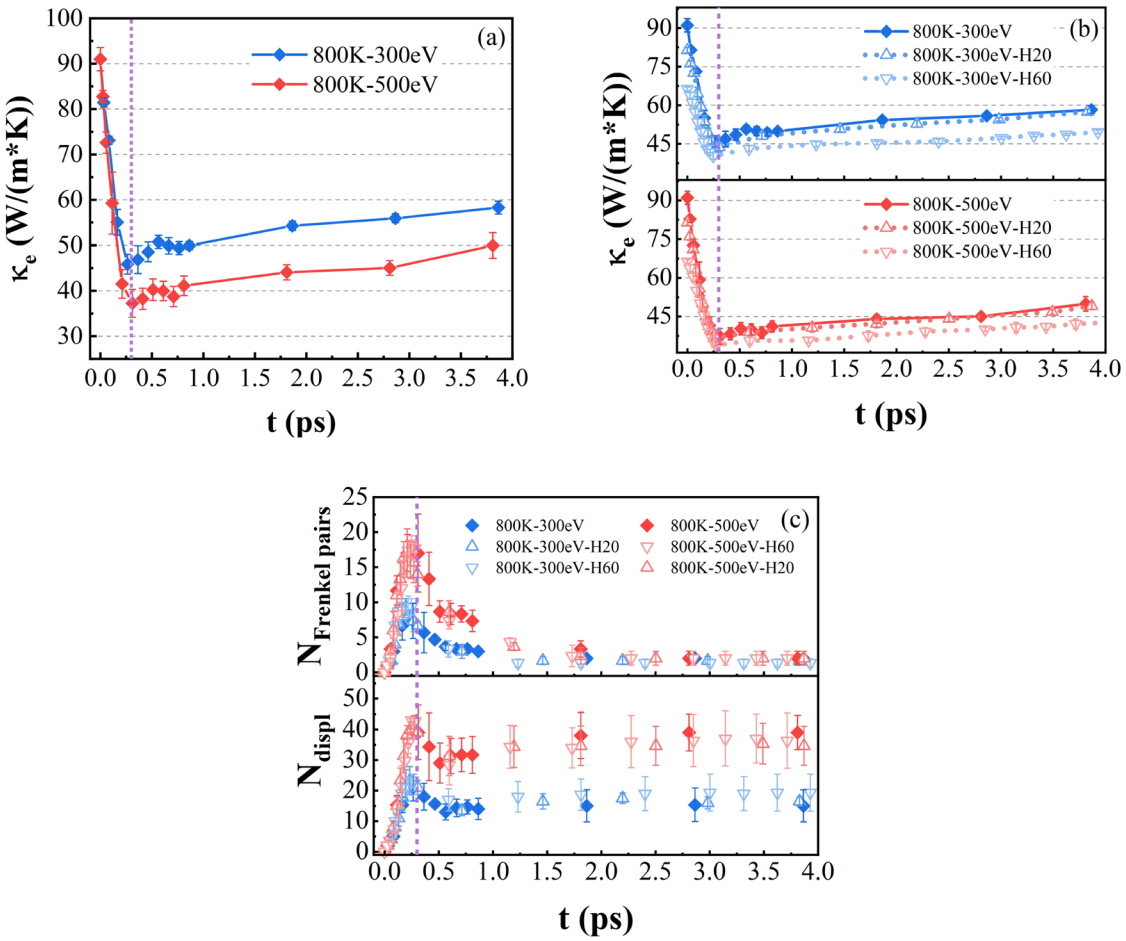

Fig. 2 (Color online) The electronic thermal conductivity of pure tungsten systems (**a**) and tungsten systems with and without H atoms (**b**) at 800 K and different E_{PKA} as a function of time during cascades. **c** The number of Frenkel pairs and displaced atoms for the considered systems at 800 K as a function of time. The purple dashed line corresponds to 0.3 ps

Similar trends in κ_e variation were observed for systems containing H atoms, as shown in Fig. 2b. In the case of the system with 20 H atoms (H concentration: 0.88%), κ_e closely resembled that of pure tungsten systems, except for a reduction of approximately 10 W m^{-1} K^{-1} at 0 ps. For systems with 60 H atoms (H concentration: 2.65%), κ_e in E_{PKA} =300 eV cascade exhibited a clear reduction compared to that of pure tungsten systems. In contrast, the reduction in κ_e in the E_{PKA}=500 eV cascade appeared to be less significant. This suggests that a high concentration of H atoms in tungsten can further reduce κ_e, particularly in low-energy cascades. Additionally, the rates of reduction and recovery in κ_e for H-containing systems are lower than those for pure tungsten systems, as reflected by the slopes of the curves in Fig. 2b.

To gain a deeper understanding of the variations in κ_e, we examined the numbers of displaced atoms and Frenkel pairs. We focused on the defects associated with W atoms for a clear comparison between systems with and without H atoms. As shown in Fig. 2c, the numbers of both defects first sharply increase and then reach local maxima at 0.3 ps. Subsequently, the number of Frenkel pairs gradually decreases and approaches zero, after which the number of displaced atoms gradually stabilizes. Furthermore, both defect numbers noticeably increase as E_{PKA} increases, whereas the introduction of H atoms has little effect on these quantities, indicating that the reduction in κ_e may be attributed to the H atom itself. The behavior of these defect variations roughly matches the κ_e behavior because an increase in the defect numbers enhances electron scattering and ultimately degrades the electronic transport performance. However, it is worth noting that although the number of Frenkel pairs approaches zero after 2 ps, the corresponding κ_e value remains close to its minimum and is significantly lower than the value at 0 ps. This suggests that despite the decrease in the number of vacancies and interstitials, the electrons in the system continue to experience severe scattering. In this scenario, we speculate that the severe electron scattering

is due to the accumulation of slight structural distortions. These distortions likely arise from the incomplete restoration of displaced atoms to their initial thermal equilibrium state within a few picoseconds during the recombination of the point defects.

To validate this hypothesis, we extracted the centrosymmetry parameter (P) for each W atom in the systems. This parameter qualifies the deviation from centrosymmetry in the immediate vicinity of an atom. Table 1 presents representative data for both pure tungsten systems and systems containing 60 H atoms, where E_{PKA} is 500 eV. Initially (at 0 ps), approximately 2.12% of the W atoms in pure tungsten exhibit P values greater than 1, indicating significant deviations from centrosymmetry in the immediate vicinity of only a few atoms due to atomic thermal motion. As the cascade event progresses, the structural evolution leads to changes in the number of W atoms, with P values greater than 1. At approximately 4 ps, the number of W atoms with P values above 1 is slightly lower than that at approximately 0.3 ps but remains significantly higher than that at the initial thermal equilibrium state (0 ps). This indicates that a few picoseconds after the PKA incidents, the local environment of some W atoms still substantially deviates from the thermal equilibrium state. The accumulation of these deviations can result in strong electron scattering, as evidenced by a 1.66 nm decrease in MFP around 4 ps compared to the initial state (0 ps). When 60 H atoms are present in the system, two notable differences emerge in the analysis of centrosymmetry parameters. First, the presence of H atoms exacerbates the deviation from centrosymmetry near the W atoms. Second, the rate of change of Psum decreases when H atoms are present. These differences are consistent with the observed alterations in κ_e.

3.2 Effect of temperature on electronic thermal conductivity

It is widely acknowledged that the influence of temperature on defect generation during a cascade is relatively minor [43]. However, the effect of temperature on κ_e values of defective systems is complex [44]. To further investigate the impact of temperature on κ_e during cascades, we studied the κ_e values of tungsten systems with varying E_{PKA} and different numbers of H atoms under a high temperature of 1300 K.

As shown in Fig. 3a, an increase in temperature leads to a noticeable improvement in κ_e values throughout the considered cascades. Specifically, at 0.3 ps, the corresponding minimum κ_e values for all examined systems exhibit a relatively high value of approximately 50 W m^{-1} K^{-1}. Subsequently, κ_e values are consistently significantly higher than those observed at 800 K. In addition, the disparity in κ_e between the pure tungsten system and the tungsten system containing H atoms remains nearly unchanged with increasing temperature, except at 0 ps. At 0 ps, κ_e of the pure tungsten system remains almost constant, whereas that of the system with H atoms shows a significant improvement.

A count of typical defects in the cascades at 1300 K was performed, as illustrated in Fig. 3b. It was observed that the local maxima for both types of defects slightly increase compared to those at 800 K (Fig. 2c). After approximately 2 ps, the defect counts at both temperatures become similar. Moreover, Table 2 provides representative data on the CSP and MFP for the pure tungsten system and the system containing 60 H atoms at 1300 K with an E_{PKA} value of 500 eV. The major distinction between the two temperature cases lies in the significant increase in the number of W atoms with P values greater than 1 and the corresponding Psum throughout the entire process with increasing temperature. This indicates that an elevated temperature causes a greater deviation from centrosymmetry in the immediate vicinity of the W atoms, leading to enhanced electron scattering. However, the thermal transport properties of the electrons are enhanced at 1300 K compared to those at 800 K. This phenomenon arises from the complex effect of temperature on κ_e. On the one hand, a temperature rise strengthens the thermal motion of atoms, thereby augmenting the electron scattering, as supported by the CSP and MFP analyses; on the other hand, the energy carried by electrons also increases with a higher temperature, directly facilitating heat transport. The complex effect of temperature is also reflected in the Wiedemann-Franz law [45], as discussed in our previous work [44].

Table 1 Representative data of CPS and MFP for pure tungsten systems and tungsten systems with 60 H atoms with an value of 500 eV and a temperature of 800 K

Time		0 ps	0.15 ps	0.3 ps	4 ps
Pure	Number of W atoms with $P > 1$	48	283	502	384
	Summation of $P > 1$ (Psum)	268.30	1846.24	3571.75	2096.01
	Change rate of Psum	–	5.88	12.31	6.81
	Average electron MFP	3.77	2.03	1.50	2.11
60 H atoms	Number of W atoms with $P > 1$	129	350	533	516
	Summation of $P > 1$ (Psum)	789.78	2337.96	3722.90	2809.53
	Change rate of Psum	–	1.96	3.71	2.56
	Average electron MFP	2.76	1.66	1.32	1.52

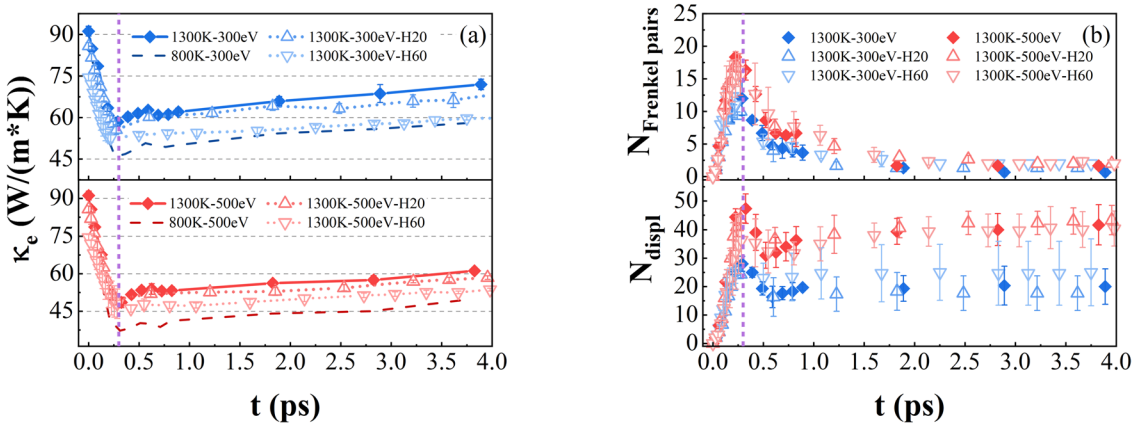

Fig. 3 (Color online) The electronic thermal conductivity (**a**) and number of Frenkel pairs and displaced atoms (**b**) of tungsten systems with and without H atoms at 1300 K and different E_{PKA} as a function of time during cascades. The purple dashed line corresponds to 0.3 ps. For comparison, the blue and red dashed lines in (**a**) correspond to the electronic thermal conductivities of pure tungsten systems at 800 K

Table 2 Representative data of CPS and MFP for pure tungsten systems and tungsten systems with 60 H atoms with an E_{PKA} value of 500 eV and a temperature of 1300 K

Time		0 ps	0.23 ps	0.3 ps	4 ps
Pure	Number of W atoms with $P > 1$	414	888	1015	955
	Summation of $P > 1$ (Psum)	2290.73	5555.25	6630.40	5319.31
	Change rate of Psum	–	1.43	1.89	1.32
	Average electron MFP	2.18	1.10	0.99	1.32
60 H atoms	Number of W atoms with $P > 1$	504	928	1054	991
	Summation of $P > 1$ (Psum)	2676.19	5918.74	6910.15	5562.22
	Change rate of Psum	–	1.21	1.58	1.08
	Average electron MFP	1.69	0.96	0.91	1.11

In summary, although an increase in temperature has a slight effect on defect production and even enhances electron scattering, the accompanying increase in the energy carried by electrons significantly improves electronic thermal transport.

3.3 Effect of grain boundary on electronic thermal conductivity

Previous studies [16, 20] have demonstrated that GBs can serve as effective sinks for point defects, particularly interstitials, leading to self-healing of irradiation damage. Additionally, the extent of overlap between the cascade center and the GB is known to influence the absorption effect of the GB for point defects [17, 19, 22], which may affect the electron transport properties. Hence, we examined the influence of different levels of overlap between the cascade center and the GB on κ_e during cascades. We employed a common symmetric tilt GB in W, $\sum 5[001](130)$ (Fig. 1b). In our treatment, E_{PKA} was 500 eV and the temperature was 800 K. When a PKA (green sphere in Fig. 1b) was situated near the GB, the majority of the cascades occurred within the GB plane. Conversely, when the PKA (yellow sphere in Fig. 1b) was far from the GB, only a small portion of the cascade edge overlapped with the GB plane.

Then, we calculated the κ_e values for systems with a specific GB during the cascades. Because the GB exhibited anisotropy, we extracted κ_e values separately along the X, Y, and Z directions. Figure 4a shows a substantial reduction in κ_e values in all three directions compared to the cases of the pure tungsten systems throughout the cascades. In particular, κ_e in the Y direction experienced the most pronounced decrease, primarily due to the strong electron scattering at the GB interface. Throughout the cascades, the presence of the GB itself reduced the electronic transport properties (0 ps), and the reduction (0 ps–0.3 ps) and subsequent recovery (0 ps–4 ps) of κ_e were relatively slow compared to those in the pure tungsten systems. Notably, the degree of overlap between the cascade center and GB does not significantly affect κ_e for the considered systems.

To better understand the variation of κ_e, we counted the numbers of vacancies and interstitials outside the GB. Throughout the cascades, the vacancies outnumbered the interstitials for both degrees of overlap between the

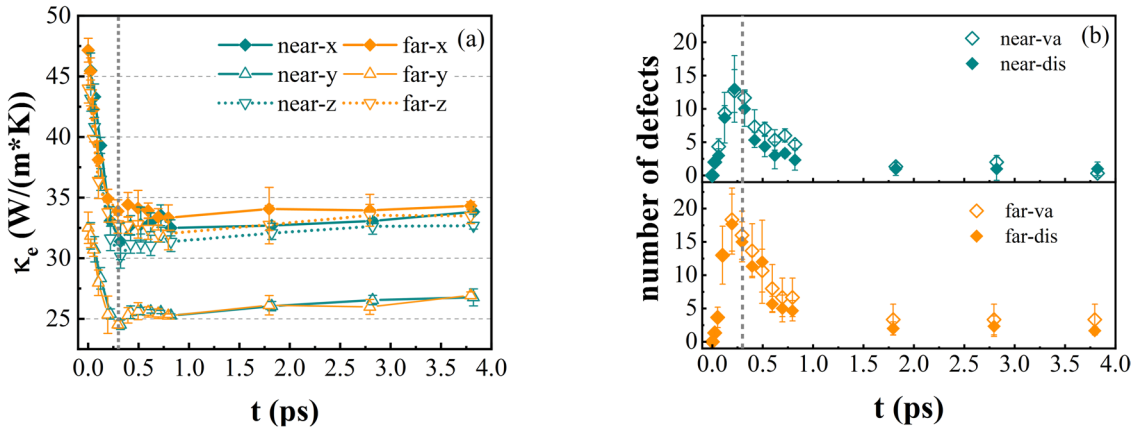

Fig. 4 (Color online) The electronic thermal conductivity (**a**) and number of vacancies and interstitials in grain interior (**b**) of GB systems with different overlap degrees of the GB and cascade center at 800 K as a function of time during cascades. The green symbols correspond to the case in which the PKA is near the GB, and the yellow symbols correspond to the case in which the PKA is far from the GB. The gray vertical dashed line corresponds to 0.3 ps

cascade center and GB. Moreover, increasing the degree of overlap decreased the number of vacancies and interstitials outside the GB. These results were consistent with those of previous studies [17, 19, 22]. However, the enhancement in the absorption effect of the GB does not improve κ_e but rather slightly weakens it at approximately 0.3 ps in the *X* and *Z* directions. This indicates that point defects absorbed by the GB continue to negatively impact electronic transport in the short term, despite reducing the defects within the grain interior. The corresponding data in Table 3 for both cases support this observation. Specifically, similar CSP data and comparable MFP for the two cases indicate similar deviations from centrosymmetry in the immediate vicinity of the atoms and comparable electron scattering intensities.

3.4 Discussion on using TB model for calculation

First, we highlight the reliability of the WHTB potential model for calculating the electronic thermal conductivities of tungsten-based systems. In this work, electronic thermal conductivity was obtained based on electrical conductivity through the Kubo-Greenwood method; therefore, an accurate calculation of electrical conductivity is crucial. Reference [46] compared the electrical conductivities of pristine tungsten calculated using the WTB potential model (on which the WHTB potential is based) and measured experimentally at different temperatures. Notably, a favorable alignment between the theoretical and experimental values at high temperatures ($T \geq 800$ K) was observed for pristine tungsten. However, at low temperatures, the TB model underestimates electrical conductivity. This is because the impact of long-range electron interactions increases as the

Table 3 The representative data of CPS and MFP for GB systems with different overlap degrees of the GB and cascade center with an E_{PKA} value of 500 eV and a temperature of 800 K

Time			0 ps	0.2 ps	0.3 ps	4 ps
Cascade center overlaps with GB	Number of W atoms with $P > 1$		404	827	894	921
	Summation of $P > 1$ (Psum)		3431.19	6286.75	6764.72	6221.36
	Change rate of Psum		–	0.83	0.97	0.81
	Average electron MFP	*X*	1.94	1.23	1.18	1.26
		Y	1.27	0.91	0.87	0.96
		Z	1.73	1.13	1.08	1.18
Cascade edge overlaps with GB	Number of W atoms with $P > 1$		404	871	933	899
	Summation of $P > 1$ (Psum)		3431.19	6586.79	6858.80	6133.09
	Change rate of Psum		–	0.92	1.00	0.79
	Average electron MFP	*X*	1.94	1.31	1.26	1.29
		Y	1.27	0.90	0.89	1.01
		Z	1.73	1.22	1.19	1.23

temperature decreases, and the TB model cannot deal with these interactions well.

A similar underestimation is evident in the calculations of the electronic thermal conductivity of pristine tungsten systems, and this underestimation also intensifies with decreasing temperature. However, it is noted that the referenced work compared the electronic thermal conductivity calculated by the Kubo-Greenwood method and the total thermal conductivity measured directly in experiments, with the latter including not only the electronic thermal conductivity but also the lattice thermal conductivity. Hence, some of the underestimation stems from the absence of the lattice thermal conductivity. In experiments, electronic thermal conductivity can be indirectly determined by measuring the electrical conductivity and applying the Wiedemann-Franz law [47]. In our previous work [44], we conducted a comparative analysis of the electronic thermal conductivity of pristine tungsten at 800 K obtained by TB calculations and experiments. The respective values were 95.92 W m^{-1} K^{-1} and 102.36 W m^{-1} K^{-1}, which are close to each other. Therefore, the electronic thermal conductivity data for tungsten-based systems at high temperatures ($T \geq 800$ K) obtained using the WHTB potential model can be considered reliable.

Next, we discuss the significance of our investigation using the TB model. In this study, we focused on the dynamic evolution of the electronic thermal conductivity of tungsten during the displacement cascade process under diverse conditions, which is difficult to directly measure experimentally. This process corresponds to the early stage of neutron irradiation, leading to the generation of a significant number of vacancies and interstitials in the materials within a brief timeframe at the picosecond level. The resulting alterations in the thermal transport properties are substantial, potentially affecting the normal service of PFM. Hence, the electronic thermal conductivity variation in tungsten during the cascade process must be investigated. Currently, research on the electronic thermal conductivity of tungsten during cascade processes is limited because of the difficulty of handling electronic structures in large and complex systems. Although the WHTB model can be used to determine the electronic thermal conductivity of tungsten under low-energy cascades, it is difficult to directly compare the results with the conductivities of materials experiencing high-energy and sustained neutron irradiation at the macroscopic level. Nevertheless, our research contributes to this field in two ways. First, the results reveal the influence of diverse cascade conditions on the electronic thermal conductivity of tungsten; second, our study can provide foundational data for simulations using the phase-field model, facilitating simulations that more accurately reflect the actual evolution of thermal transport properties of tungsten under neutron irradiation.

4 Conclusion

In conclusion, we employed the WHTB model and the Kubo-Greenwood method to investigate how PKA energy, H atoms, temperature, and GB affect κ_e of tungsten systems during collision cascades. Our findings revealed a rapid reduction in κ_e within the initial 0.3 ps, followed by a gradual recovery. A higher PKA energy and high concentration of H atoms worsen the reduction in κ_e during the cascades. With increasing temperature, κ_e shows a significant improvement during cascades due to the increased energy carried by electrons, despite exhibiting fewer changes in defect production and an apparent enhancement in electron scattering. The presence of the considered GB has a notable negative impact on κ_e, and the absorption of point defects by GB does not improve the κ_e performance. In addition, the evolution of the defect count approximately matched the changes in κ_e, whereas the accumulation of microstructural distortion keeps κ_e relatively low when the number of point defects approaches zero.

Acknowledgements The computational center of USTC and Hefei Advanced Computing Center are acknowledged for computational support.

Author contributions All authors contributed to the study conception and design. Material preparation, data collection and analysis were performed by Jiong-Rong Wang and Bi-Cai Pan. The first draft of the manuscript was written by Jiong-Rong Wang and all authors commented on previous versions of the manuscript. All authors read and approved the final manuscript.

Data availability The data that support the findings of this study are openly available in Science Data Bank at https://cstr.cn/31253.11.sciencedb.j00186.00362 and https://www.doi.org/10.57760/sciencedb.j00186.00362.

Declarations

Conflict of interest The authors declare that they have no Conflict of interest.

References

1. Y.C. Chen, J.Z. Fang, L.X. Liu et al., The interactions between rhenium and interstitial-type defects in bulk tungsten: a combined study by molecular dynamics and molecular statics simulations. J. Nucl. Mater. **522**, 200–211 (2019). https://doi.org/10.1016/j.jnucmat.2019.05.003
2. X.O. Yi, L. Zhang, W.T. Han et al., Defect characterization, mechanical and thermal property evaluation in CVD-W after low-dose neutron irradiation. Int. J Refract. Hard. Met. **85**, 105004 (2019). https://doi.org/10.1016/j.ijrmhm.2019.105004
3. X.P. Li, H.Y. Fan, W.F. Liu et al., The heat flux and temperature distribution of W fuzz layers under fusion-relevant He/D ion irradiations. J. Nucl. Mater. **557**, 153319 (2021). https://doi.org/10.1016/j.jnucmat.2021.153319

4. S.L. Qu, H. Sun, A. Kreter et al., Degradation of thermal conductivity of the damaged layer of tungsten irradiated by helium-plasma. Fusion Eng. Des. **137**, 97–103 (2018). https://doi.org/10.1016/j.fusengdes.2018.08.014
5. K. Nordlund, C. Bjorkas, T. Ahlgren et al., Multiscale modelling of plasma-wall interactions in fusion reactor conditions. J. Phys. D **47**(22), 224018 (2014). https://doi.org/10.1088/0022-3727/47/22/224018
6. T.D. de la Rubia, H.M. Zbib, T.A. Khraishi et al., Multiscale modelling of plastic flow localization in irradiated materials. Nature **406**, 871–874 (2000). https://doi.org/10.1038/35022544
7. S. Cui, R.P. Doerner, M.J. Simmonds et al., Thermal conductivity degradation and recovery in ion beam damaged tungsten at different temperature. J. Nucl. Mater. **511**, 141–147 (2018). https://doi.org/10.1016/j.jnucmat.2018.09.002
8. J. Habainy, Y. Dai, Y. Lee et al., Thermal diffusivity of tungsten irradiated with protons up to 5.8 dpa. J. Nucl. Mater. **509**, 152–157 (2018). https://doi.org/10.1016/j.jnucmat.2018.06.041
9. Y. Katoh, L.L. Snead, L.M. Garrison et al., Response of unalloyed tungsten to mixed spectrum neutrons. J. Nucl. Mater. **520**, 193–207 (2019). https://doi.org/10.1016/j.jnucmat.2019.03.045
10. G.R. Tynan, R.P. Doerner, J. Barton et al., Deuterium retention and thermal conductivity in ion-beam displacement-damaged tungsten. Nucl. Mater. Energy **12**, 164–168 (2017). https://doi.org/10.1016/j.nme.2017.03.024
11. Y. Chen, K.Y. Yu, Y. Liu et al., Damage-tolerant nanotwinned metals with nanovoids under radiation environments. Nat. Commun. **6**, 7036 (2015). https://doi.org/10.1038/ncomms8036
12. D.R. Mason, A.E. Sand, X. Yi et al., Direct observation of the spatial distribution of primary cascade damage in tungsten. Acta Mater. **144**, 905–917 (2018). https://doi.org/10.1016/j.actamat.2017.10.031
13. X. Yi, A.E. Sand, D.R. Mason et al., Direct observation of size scaling and elastic interaction between nano-scale defects in collision cascades. Epl **110**(3), 36001 (2015). https://doi.org/10.1209/0295-5075/110/36001
14. W. Setyawan, G. Nandipati, K.J. Roche et al., Displacement cascades and defects annealing in tungsten, part I: defect database from molecular dynamics simulations. J. Nucl. Mater. **462**, 329–337 (2015). https://doi.org/10.1016/j.jnucmat.2014.12.056
15. X.D. Yang, H.Q. Deng, N.W. Hu et al., Molecular dynamics simulation of the displacement cascades in tungsten with interstitial helium atoms. Fusion Sci. Technol. **66**(1), 112–117 (2014). https://doi.org/10.13182/fst13-742
16. X.Y. Li, W. Liu, Y.C. Xu et al., An energetic and kinetic perspective of the grain-boundary role in healing radiation damage in tungsten. Nucl. Fusion **53**(12), 123014 (2013). https://doi.org/10.1088/0029-5515/53/12/123014
17. H. Li, Y. Qin, Y.Y. Yang et al., The evolution of interaction between grain boundary and irradiation-induced point defects: symmetric tilt GB in tungsten. J. Nucl. Mater. **500**, 42–49 (2018). https://doi.org/10.1016/j.jnucmat.2017.12.013
18. X.Y. Wang, N. Gao, W. Setyawan et al., Effect of irradiation on mechanical properties of symmetrical grain boundaries investigated by atomic simulations. J. Nucl. Mater. **491**, 154–161 (2017). https://doi.org/10.1016/j.jnucmat.2017.04.051
19. C.G. Zhang, W.H. Zhou, Y.G. Li et al., Primary radiation damage near grain boundary in bcc tungsten by molecular dynamics simulations. J. Nucl. Mater. **458**, 138–145 (2015). https://doi.org/10.1016/j.jnucmat.2014.11.135
20. X.M. Bai, A.F. Voter, R.G. Hoagland et al., Efficient annealing of radiation damage near grain boundaries via interstitial Emission. Science **327**(5973), 1631–1634 (2010). https://doi.org/10.1126/science.1183723
21. J.H. Zhang, H. He, W.B. Liu et al., Effects of grain boundaries on the radiation-induced defects evolution in BCC Fe-Cr alloy: a molecular dynamics study. Nucl. Mater. Energy **22**, 100726 (2020). https://doi.org/10.1016/j.nme.2020.100726
22. A. Esfandiarpour, S.A.H. Feghhi, A.A. Shokri, Effects of atomic grain boundary structures on primary radiation damage in alpha-Fe. Nucl. Instrum. Methods Phys. Res. B **362**, 1–8 (2015). https://doi.org/10.1016/j.nimb.2015.08.074
23. Y.Y. Wang, J.J. Zhao, Numerical simulations of thermal conductivity in void-containing tungsten: topological feature of voids. J. Nucl. Mater. **543**, 152601 (2021). https://doi.org/10.1016/j.jnucmat.2020.152601
24. Y.Y. Wang, J.J. Zhao, Understanding the thermal conductivity of pristine W and W-Re alloys from a physics-based model. J. Nucl. Mater. **529**, 151931 (2020). https://doi.org/10.1016/j.jnucmat.2019.151931
25. L. Hu, B.D. Wirth, D. Maroudas, Thermal conductivity of tungsten: effects of plasma-related structural defects from molecular-dynamics simulations. Appl. Phys. Lett. **111**(8), 081902 (2017). https://doi.org/10.1063/1.4986956
26. H.Y. Zhang, J.Z. Sun, Y.M. Wang et al., Study of lattice thermal conductivity of tungsten containing bubbles by molecular dynamics simulation. Fusion Eng. Des. **161**, 112004 (2020). https://doi.org/10.1016/j.fusengdes.2020.112004
27. Y.M. Ding, X.B. Wu, J. Zhan et al., Simulation study of effects of grain boundary and helium bubble on lattice thermal resistance of tungsten. Fusion Eng. Des. **168**, 112682 (2021). https://doi.org/10.1016/j.fusengdes.2021.112682
28. Q. Wang, N. Gui, X.L. Huang et al., The effect of temperature and cascade collision on thermal conductivity of 3C-SiC: a molecular dynamics study. Int. J. Heat Mass Transf. **180**, 121822 (2021). https://doi.org/10.1016/j.ijheatmasstransfer.2021.121822
29. X.N. Huang, J. Guo, Y.N. Yue, Graphene coated 3C-SiC with improved irradiation resistance and enhanced heat conduction property after collision cascade. Int. J. Heat Mass Transf. **194**, 122988 (2022). https://doi.org/10.1016/j.ijheatmasstransfer.2022.122988
30. J.R. Wang, X.B. Ye, W.Y. Ding et al., Interplay between the edge dislocation and hydrogen in tungsten at electronically excited states. Adv. Phys. Res. **2**(8), 2200115 (2023). https://doi.org/10.1002/apxr.202200115
31. H.J.C. Berendsen, J.P.M. Postma, W.F. Vangunsteren et al., Molecular-dynamics with coupling to an external bath. J. Chem. Phys. **81**(8), 3684–3690 (1984). https://doi.org/10.1063/1.448118
32. K. Nordlund, Molecular dynamics simulation of ion ranges in the 1–100 keV energy range. Comput. Mater. Sci. **3**(4), 448–56 (1995). https://doi.org/10.1016/0927-0256(94)00085-q
33. R. Kubo, Statistical-mechanical theory of irreversible processes. I. general theory and simple applications to magnetic and conduction problems. J. Phys. Soc. Jpn. **12**(6), 570–586 (1957). https://doi.org/10.1143/JPSJ.12.570
34. M. Onoda, N. Nagaosa, Topological nature of anomalous hall effect in ferromagnets. J. Phys. Soc. Jpn. **71**(1), 19–22 (2002). https://doi.org/10.1143/JPSJ.71.19
35. K. Nomura, A.H. MacDonald, Quantum transport of massless dirac fermions. Phys. Rev. Lett. **98**(7), 076602 (2007). https://doi.org/10.1103/PhysRevLett.98.076602
36. V. Recoules, J.P. Crocombette, Ab initio determination of electrical and thermal conductivity of liquid aluminum. Phys. Rev. B **72**(10), 104202 (2005). https://doi.org/10.1103/PhysRevB.72.104202
37. G.V. Chester, A. Thellung, The law of wiedemann and franz. Proc. Phys. Soc. **77**(5), 1005 (1961). https://doi.org/10.1088/0370-1328/77/5/309
38. F. Triozon, S. Roche, A. Rubio et al., Electrical transport in carbon nanotubes: role of disorder and helical symmetries. Phys. Rev. B **69**(12), 121410 (2004). https://doi.org/10.1103/PhysRevB.69.121410

39. T. Markussen, R. Rurali, M. Brandbyge et al., Electronic transport through Si nanowires: role of bulk and surface disorder. Phys. Rev. B **74**(24), 245313 (2006). https://doi.org/10.1103/PhysRevB.74.245313
40. T.M. Radchenko, A.A. Shylau, I.V. Zozoulenko et al., Effect of charged line defects on conductivity in graphene: numerical Kubo and analytical Boltzmann approaches. Phys. Rev. B **87**(19), 195448 (2013). https://doi.org/10.1103/PhysRevB.87.195448
41. K. Nordlund, M. Ghaly, R.S. Averback et al., Defect production in collision cascades in elemental semiconductors and fcc metals. Phys. Rev. B **57**(13), 7556–7570 (1998). https://doi.org/10.1103/PhysRevB.57.7556
42. C.L. Kelchner, S.J. Plimpton, J.C. Hamilton, Dislocation nucleation and defect structure during surface indentation. Phys. Rev. B **58**(17), 11085–11088 (1998). https://doi.org/10.1103/physrevb.58.11085
43. D.J. Bacon, F. Gao, Y.N. Osetsky, The primary damage state in fcc, bcc and hcp metals as seen in molecular dynamics simulations. J. Nucl. Mater. **276**, 1–12 (2000). https://doi.org/10.1016/s0022-3115(99)00165-8
44. J.R. Wang, D.H. Zhu, J.L. Chen et al., Effect of lattice defects, hydrogen impurity and temperature on electronic thermal conductivity in first wall tungsten materials. J. Nucl. Mater. **581**, 154418 (2023). https://doi.org/10.1016/j.jnucmat.2023.154418
45. N. Stojanovic, D.H.S. Maithripala, J.M. Berg et al., Thermal conductivity in metallic nanostructures at high temperature: electrons, phonons, and the Wiedemann-Franz law. Phys. Rev. B **82**(7), 075418 (2010). https://doi.org/10.1103/PhysRevB.82.075418
46. Z.H. He, X.B. Ye, W.Y. Ding et al., An empirical law on the finite-size effects in electronic transport calculations of tungsten. AIP Adv. **9**(9), 095047 (2019). https://doi.org/10.1063/1.5123548
47. T. Tanabe, C. Eamchotchawalit, C. Busabok et al., Temperature dependence of thermal conductivity in W and W-Re alloys from 300 to 1000 K. Mater. Lett. **57**(19), 2950–2953 (2003). https://doi.org/10.1016/s0167-577x(02)01403-9